RESEARCH ARTICLE

LASER & PHOTONICS REVIEWS

www.lpr-journal.org

Near-Field Coupling of Janus Dipoles Beyond Polarization Locking

Chan Wang, Yuhan Zhong, Xuhuinan Chen, Huaping Wang, Tony Low,* Hongsheng Chen, Baile Zhang, and Xiao Lin**

Polarization, as a fundamental property of light, plays a key role in many phenomena of near-field coupling, namely the coupling of source's evanescent waves into some guided modes. As a typical example of the polarization-locked phenomenon in the near-field coupling, the Janus dipole has the orientation of its near-field coupling face intrinsically determined by the polarization state of linearly-polarized surface waves, specifically whether they are transverse-magnetic (TM) or transverse-electric (TE) surface waves. Here, a mechanism to achieve the directional near-field coupling of Janus dipoles beyond polarization locking by leveraging hybrid TM-TE surface waves is presented. These hybrid surface waves, as eigenmodes with both TM and TE wave components, can be supported by optical interfaces between different filling materials inside a parallel-plate waveguide. Under the excitation of hybrid surface waves, it is found that the coupling and non-coupling face of a Janus dipole may be switched, if the Janus dipole itself rotates in a plane parallel to the designed optical interface between different filling materials, without resorting to the change of surface-wave polarization. The underlying mechanism is due to the capability of hybrid surface waves to extract both the source's TM and TE evanescent waves, which offers an alternative paradigm to regulate the interference in the near-field coupling.

1. Introduction

Polarization, an inherent property of light, significantly enriches the physics of light-matter interactions. It offers an amenable route to molding the flow of light and especially manipulation of near-field coupling,[1–8] including the coupling directionality and coupling strength. The phenomena of polarization-controlled near-field coupling are key to many applications, such as near-field microscopy, [9–11] chiral quantum optics,[12–14] biomedical and clinical polarimetry,[14–17] photonic computation,[18] and nanorouters.[19–22]

The polarization of light provides two routes to tailoring the near-field coupling. One route is to control the polarization state of incident waves,[23–34] which is easily achievable in experiments. As governed by spin-momentum locking, the directionality of excited surface waves (SW) could be flipped when the handedness of the incident wave polarization

C. Wang, Y. Zhong, X. Chen, H. Chen, X. Lin
Interdisciplinary Center for Quantum Information
State Key Laboratory of Extreme Photonics and Instrumentation
Zhejiang University
Hangzhou 310027, China
E-mail: xiaolinzju@zju.edu.cn

C. Wang, H. Chen
Key Lab. of Advanced Micro/Nano Electronic Devices and Smart Systems of Zhejiang
Jinhua Institute of Zhejiang University
Zhejiang University
Jinhua 321036, China

Y. Zhong, H. Chen, X. Lin
International Joint Innovation Center
The Electromagnetics Academy at Zhejiang University
Zhejiang University
Haining 314400, China

H. Wang
Key Laboratory of Ocean Observation-Imaging Testbed of Zhejiang Province
Institute of Marine Electronics Engineering
Ocean College
Zhejiang University
Hangzhou 310027, China
E-mail: hpwang@zju.edu.cn

T. Low
Department of Electrical and Computer Engineering
University of Minnesota
Minnesota 55455, USA
E-mail: tlow@umn.edu

H. Chen
Shaoxing Institute of Zhejiang University, Zhejiang University
Shaoxing 312000, China

B. Zhang
Division of Physics and Applied Physics
School of Physical and Mathematical Sciences
Nanyang Technological University
Singapore 637371, Singapore

B. Zhang
Centre for Disruptive Photonic Technologies
Nanyang Technological University
Singapore 637371, Singapore

The ORCID identification number(s) for the author(s) of this article can be found under https://doi.org/10.1002/lpor.202301035

DOI: 10.1002/lpor.202301035

changes from the left-handed circular polarization to the right-handed one.[35–38] The other route is to control the polarization state of excited surface waves.[39–43] This route may enable the near-field directionality beyond spin-momentum locking if the complex dipoles with both the electric dipole moment $\bar{p}$ and the magnetic dipole moment $\bar{m}$ (e.g., Janus dipole) are used.[39] For example, the Janus dipole has its electric and magnetic dipole moments perpendicular to each other, but 90° out of phase, and fulfilling the Kerker condition[44] of $|\bar{p}|/|\bar{m}| = c$, where c is the speed of light in free space. Essentially, the Janus dipole has the orientation of its near-field coupling face determined by the polarization state of excited linearly-polarized surface waves, namely polarization locking. To be specific, its coupling face orientation for transverse-magnetic (TM, *p*-polarized) surface waves is always opposite to that of transverse-electric (TE, *s*-polarized) surface waves.[42] As a result, the near-field directionality of Janus dipoles could be flexibly toggled by tailoring the polarization of excited surface waves, for example, via tuning the chemical potential of graphene in a graphene-metasurface waveguide.[42]

To date, the manipulation of near-field coupling via changing the polarization state of surface waves is still in its infancy and focused primarily on linearly polarized surface waves. That is, TM and TE evanescent waves carried by the dipolar source are generally separately exploited for the manipulation of near-field coupling.[45] This is despite the fact that physical systems with surface waves without linear polarizations (e.g., hybrid TM-TE surface waves) are abundant. Hybrid TM-TE surface waves intrinsically possess both TM and TE wave components and exist widely in complex optical systems, such as those supported by anisotropic metasurfaces,[46–51] chiral surface waves (e.g., supported by moiré graphene),[52–56] Dyakonov surface waves,[57–59] ghost surface polaritons,[60] and hyperbolic shear polaritons.[61,62] Unlike linearly-polarized surface waves, these hybrid surface waves can be excited either by TM evanescent waves that the dipolar source carries or by TE ones. In other words, hybrid surface waves could offer a feasible route to utilizing both the source's TM and TE evanescent waves in the near-field coupling. This way, these hybrid surface waves may provide new opportunities in tailoring dipole-matter interactions and offer an alternative scheme for shaping the near-field coupling.

In this work, we show the possibility of engineering the directional near-field coupling via hybrid TM-TE surface waves, such as those supported by the optical interface between different filling materials inside a parallel-plate waveguide. Under the excitation of these hybrid surface waves, we reveal a phenomenon of directional near-field coupling of Janus dipoles beyond polarization locking. To be specific, we find the coupling face orientation of the Janus dipole could be flipped by rotating the Janus dipole itself in a plane parallel to the designed optical interface, without resorting to the variation of the surface-wave polarization.

2. Results and Discussion

Figure 1 conceptually illustrates the directional near-field coupling of Janus dipoles beyond polarization locking via hybrid TM-TE surface waves inside a parallel plate waveguide. This waveguide consists of two parallel perfect electric conductors (PEC) separated by a vertical distance d. In order to manifest the coupling and non-coupling faces of the Janus dipole, two parallel but spatially well-separated out-couplers are designed inside the waveguide. That is, each out-coupler supports the propagation of hybrid TM-TE surface waves and corresponds to the optical interface at $y = \pm y_0$ between nonmagnetic materials a and b with relative permittivities ε_a and ε_b, respectively. Note that the hybrid TM-TE surface waves supported by the designed interface between different filling materials inside a parallel-plate waveguide have a correlated phase/magnitude relation between their TM and TE wave components. The hybrid TM-TE surface waves are essentially different from the conventional guided modes supported by a parallel-plate waveguide, which are linearly polarized (e.g., TM_1 guided mode or TE_1 guided mode). In addition, the hybrid TM-TE surface waves studied in this work (i.e., with a correlated phase/magnitude relation between TM and TE wave components) are distinctly different from the conventional unpolarized light which generally has a random phase/magnitude relation between TM and TE wave components. Without loss of generality, the Janus dipole is composed of an electric dipole moment $\bar{p}/p_0 = \hat{x}\sin\theta + \hat{z}\cos\theta$ and a magnetic dipole moment $\bar{m}/icp_0 = \hat{x}\cos\theta - \hat{z}\sin\theta$, where $p_0 = 1\ \mathrm{C}\cdot\mathrm{m}$ and the rotation angle θ is the angle between $\bar{p}$ and $\hat{z}$. In other words, the Janus dipole rotates within the xz plane, which is parallel to our designed interfaces.

Below we analyze the near-field coupling between the Janus dipole and the designed out-couplers. To facilitate the general discussion, the Janus dipole is within the matter with a relative permittivity of ε_r and a relative permeability of μ_r. After some calculations (see supplementary section S2), the excited hybrid TM-TE surface waves at the interface of $y = \pm y_0$ could be obtained as:

$$\begin{aligned}\%E_z^{\mathrm{hybrid}}(x,\pm y_0,z) = \%\beta_1\cdot\left[-\frac{k_{x,sw}k_z}{k_{x,sw}^2+k_{y,sw}^2}\sin\theta+\left(1\pm\frac{i\varepsilon_r\mu_r k_0 k_{y,sw}}{k_{x,sw}^2+k_{y,sw}^2}\right)\cos\theta\right]\\ -\beta_2\cdot\left[\left(i\pm\frac{k_0 k_{y,sw}}{k_{x,sw}^2+k_{y,sw}^2}\right)\sin\theta+\frac{ik_{x,sw}k_z}{k_{x,sw}^2+k_{y,sw}^2}\cos\theta\right]\end{aligned} \tag{1}$$

where the subscript "sw" is the abbreviation of surface waves, $\bar{k}_{r,sw} = \hat{x}\,k_{x,sw} + \hat{y}k_{y,sw} + \hat{z}k_z$ is the wavevector of hybrid surface waves, $k_z = m\pi/d$ (m is an integer) according to the guidance condition,[63] $z \in [-d/2, d/2]$, $k_0 = \omega/c$, ε_0 is the permittivity of free space, and ω is the angular frequency. For conceptual illustration, below we only consider the excitation of the lowest-order hybrid surface waves with $m = 1$, namely $k_z = \pi/d$. Accordingly, we have $\beta_1 = \frac{\kappa}{\varepsilon_0\varepsilon_r}\cdot\mathrm{Res}[R_{TM}^{TM}(k_{x,sw})]$ and $\beta_2 = c\kappa\cdot\mathrm{Res}[R_{TE}^{TM}(k_{x,sw})]$, $\kappa = \frac{p_0(k_{x,sw}^2+k_{y,sw}^2)}{2dk_{y,sw}}(1-e^{-2ik_z z})e^{ik_{x,sw}x+ik_y y_0+ik_z z}$, where R_{TM}^{TM} and R_{TE}^{TM} are the reflection coefficients under the incidence of TM and TE guided modes, respectively. Since $|e^{ik_{x,sw}x+ik_y y_0+ik_z z}| = 1$ under the lossless condition, $|\beta_1|$ and $|\beta_2|$ are actually constants.

When the rotation angle is $\theta = 0°$ or $\theta = 90°$, Equation (1) can be reduced to:

$$E_{z,\theta=0°}^{\mathrm{hybrid}}(x,\pm y_0,z) \propto (1\pm C_1) - iC_2 \tag{2}$$

$$E_{z,\theta=90°}^{\mathrm{hybrid}}(x,\pm y_0,z) \propto (1\mp C_3) - iC_4 \tag{3}$$

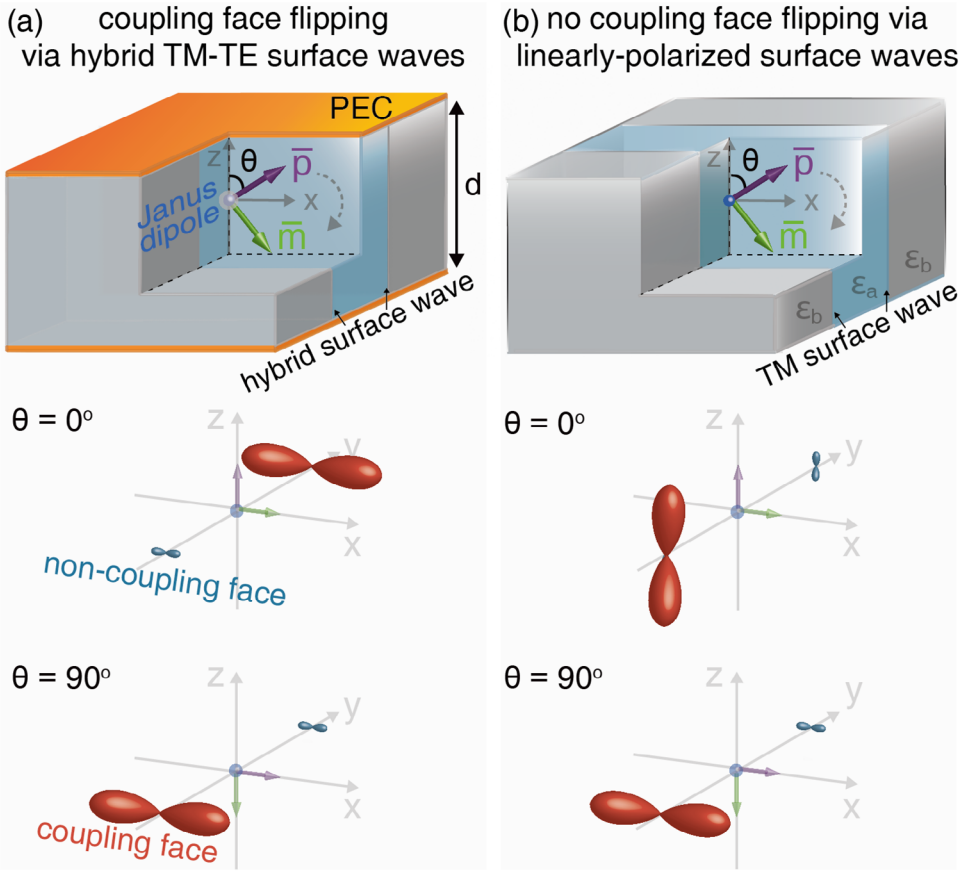

Figure 1. Conceptual illustration of near-field coupling beyond polarization locking via hybrid TM-TE surface waves inside a parallel-plate waveguide. Each optical interface between material *a* with a relative permittivity $\varepsilon_a < 0$ and material *b* with a relative permittivity $\varepsilon_b > 0$ supports the propagation of hybrid TM-TE surface waves. A Janus dipole is placed in the middle of the waveguide, and it rotates in a plane parallel to the designed optical interface. For illustration, the red conical shape schematically indicates that the evanescent waves carried by the dipolar source would mainly couple to the related out-coupler and correspond to the coupling face of the dipolar source. By contrast, the blue conical shape schematically indicates that only a bit of evanescent waves carried by the dipolar source would couple to the related out-coupler and correspond to the non-coupling face of the dipolar source. a) Schematic of coupling face flipping from $+y$ direction to $-y$ direction via hybrid surface waves if the rotation angle is changed from $\theta = 0°$ to $\theta = 90°$. b) Schematic of no coupling face flipping via linearly-polarized surface waves, if the perfect electric conductors (PEC) in (a) are removed. The linearly polarized surface waves only rotate within the *xz* plane by following the rotation of the Janus dipole itself.

where $C_1 = \frac{i\varepsilon_r\mu_r k_0 k_{y,sw}}{k_{x,sw}^2+k_{y,sw}^2}$, $C_2 = \frac{\beta_2}{\beta_1}\cdot\frac{k_{x,sw}k_z}{k_{x,sw}^2+k_{y,sw}^2}$, $C_3 = \frac{ik_0 k_{y,sw}}{k_{x,sw}^2+k_{y,sw}^2}$, and $C_4 = \frac{\beta_1}{\beta_2}\cdot\frac{k_{x,sw}k_z}{k_{x,sw}^2+k_{y,sw}^2}$ are also constants; see supplementary section S2.

If the values of C_1 and C_3 are comparable to one and the values of C_2 and C_4 are comparable to or much smaller than one, both $|E^{hybrid}_{z,\theta=0°}(x,\pm y_0,z)|^2$ and $|E^{hybrid}_{z,\theta=90°}(x,\pm y_0,z)|^2$ would be highly asymmetric regarding to y. That is, $\frac{|E^{hybrid}_{z,\theta_0}(x,+y_0,z)|^2}{|E^{hybrid}_{z,\theta_0}(x,-y_0,z)|^2} \gg 1$ or $\frac{|E^{hybrid}_{z,\theta_0}(x,+y_0,z)|^2}{|E^{hybrid}_{z,\theta_0}(x,-y_0,z)|^2} \ll 1$, no matter $\theta_0 = 0°$ or 90°. Hence, Equations (2) and (3) indicate that a Janus dipole has two near-field faces, which have distinct coupling strengths. Accordingly, the face of a Janus dipole with a relative-strong (relative-weak) coupling strength is termed as the coupling (non-coupling) face.[39,42,64]

Moreover, if $C_1C_3 > 0$ (equivalent to $\varepsilon_r\mu_r > 0$ from Equations (2) and (3)), we further have:

$$\left\{\frac{\left|E^{hybrid}_{z,\theta=0°}(x,+y_0,z)\right|^2}{\left|E^{hybrid}_{z,\theta=0°}(x,-y_0,z)\right|^2}-1\right\}\cdot\left\{\frac{\left|E^{hybrid}_{z,\theta=90°}(x,+y_0,z)\right|^2}{\left|E^{hybrid}_{z,\theta=90°}(x,-y_0,z)\right|^2}-1\right\}<0 \tag{4}$$

Equation (4) indicates that the coupling and non-coupling faces of a Janus dipole would be flipped by changing the rotation angle from 0° to 90°, as shown in Figure 1a. It is important to note that this flipping process happens along the $\pm y$ direction, while the Janus dipole itself rotates in the *xz* plane. For comparison, we also show the influence of dipolar rotation on the near-field coupling in Figure 1b when the out-coupler

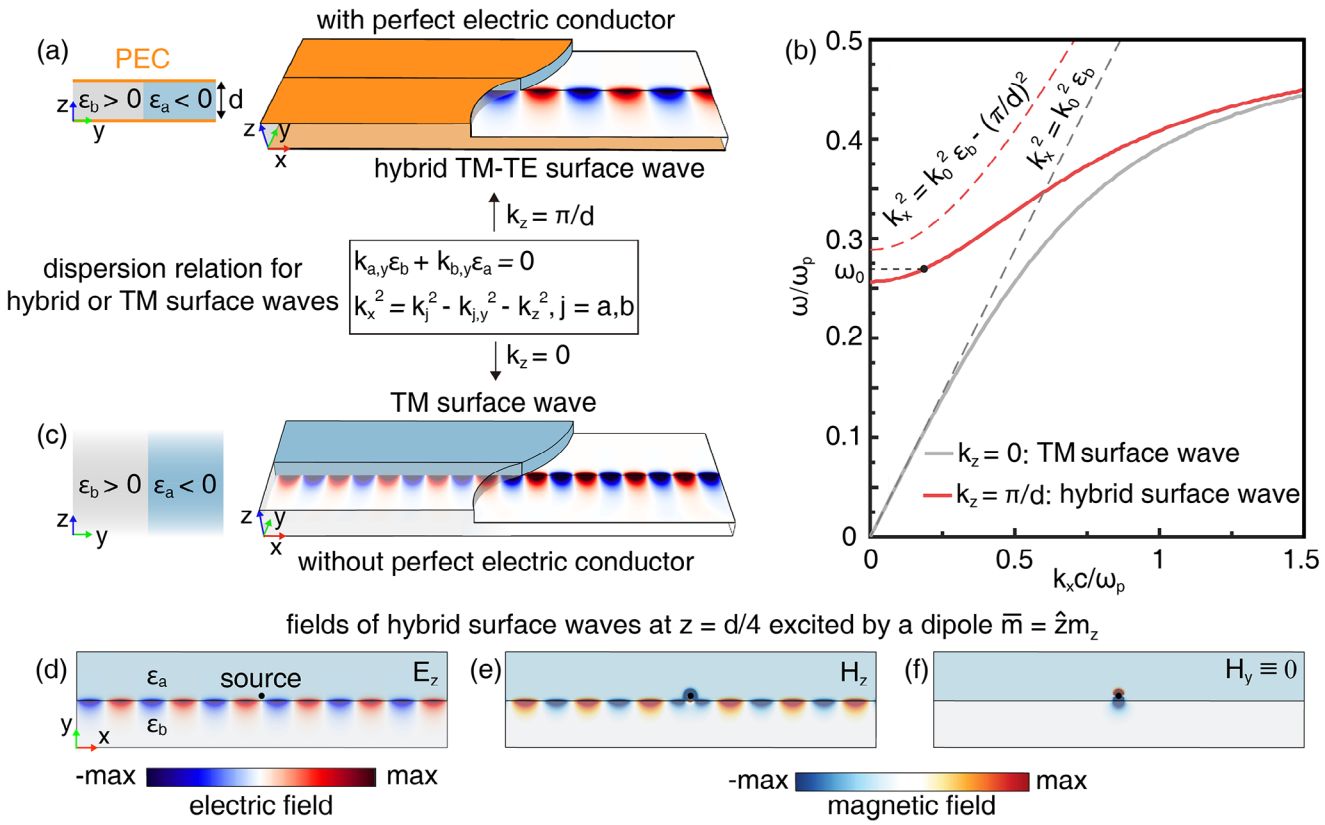

Figure 2. Hybrid surface waves supported by an optical interface between different filling materials inside a parallel-plate waveguide. a) Structural schematic of the designed optical interface, which supports the propagation of hybrid TM-TE surface waves. b) Dispersion of hybrid surface waves. For conceptual illustration, only the lowest-order hybrid surface waves (i.e., hybrid TM_1-TE_1 surface waves with $k_z = \pi/d$) are considered. In (b), $\varepsilon_b = 3$, $\varepsilon_a = 1 - \omega_p^2/\omega^2$, and $d = \lambda_p = 2\pi c/\omega_p$, where ω_p is the plasma frequency. c) Structural schematic of an optical interface supporting the propagation of TM surface waves. If TM surface waves propagate along the x direction, we have $k_z = 0$. d–f) Fields of excited hybrid surface waves at the frequency $\omega_0 = 0.27\omega_p$.

supports linearly polarized surface waves. Under this scenario, the orientation of the coupling face remains unchanged for an arbitrary rotation angle, as shown in Figure 1b. Actually, the coupling face only rotates within the xz plane by following the rotation of the Janus dipole itself.

Due to the significant role of hybrid TM-TE surface waves in regulating the near-field coupling, we now delve into their fundamental properties in **Figure 2**. By enforcing the boundary conditions, the dispersion relation of the lowest-order hybrid TM-TE surface waves at the interface between materials a and b inside the parallel-plate waveguide is governed by:

$$\left(k_{a,y}k_{b,xy}^2\mu_a + k_{b,y}k_{a,xy}^2\mu_b\right)\left(k_{a,y}k_{b,xy}^2\varepsilon_a + k_{b,y}k_{a,xy}^2\varepsilon_b\right) + \left[k_{x,sw}k_z k_0\left(\mu_a\varepsilon_a - \mu_b\varepsilon_b\right)\right]^2 = 0 \quad (5)$$

where $k_{j,xy} = \sqrt{k_j^2 - k_z^2}$, $k_{j,y} = \sqrt{k_{j,xy}^2 - k_{x,sw}^2}$, $k_z = \pi/d$, $k_j = |\bar{k}_j|$ is the amplitude of the wavevector in material a or b, $j = a$ or b, and the relative permeabilities are $\mu_a = \mu_b = 1$ for nonmagnetic materials. After some calculations, Equation (5) can be simplified to:

$$k_{a,y}\varepsilon_b + k_{b,y}\varepsilon_a = 0 \quad (6)$$

Coincidently, Equation (6) also represents the dispersion of TM surface waves supported by the interface between materials a and b in the absence of two perfect electric conductors. In short, Equation (6) governs both the dispersion of these hybrid TM-TE surface waves with $k_z = \pi/d$ and TM surface waves with $k_z = 0$. Such a coincidence actually has not been reported before.

According to Equation (6), the dispersion relations of lowest-order hybrid surface waves and TM surface waves are compared in Figure 2b, while setting $\varepsilon_b = 3$, $\varepsilon_a = 1 - \omega_p^2/\omega^2$, and $d = 2\pi c/\omega_p$, where ω_p is the plasma frequency of material a. First, the dispersion line for hybrid surface waves is always above that of TM surface waves. That is, for a given frequency, the wavelength of hybrid surface waves is larger than that of TM surface waves. Second, as the frequency increases, the two dispersion lines tend to converge, since the influence of k_z (whether $k_z = \pi/d$ or $k_z = 0$) on the shape of these dispersion lines becomes weaker for a larger $k_{x,sw}$. Third, part of the dispersion line for hybrid surface waves could extend above the light line for material b, while the dispersion line of TM surface waves is always below this light line.

We further find that these lowest-order hybrid surface waves are always featured with a zero component of magnetic field nor-

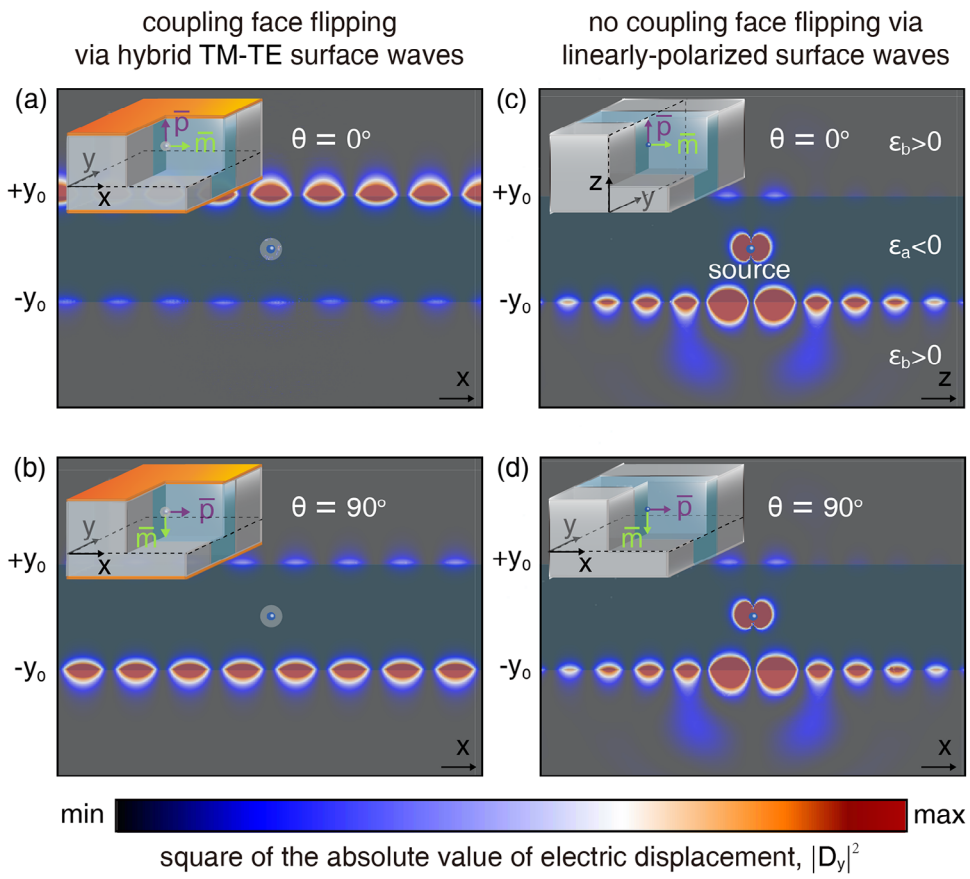

Figure 3. Flipping the coupling and non-coupling faces via hybrid TM-TE surface waves by rotating the Janus dipole in a plane parallel to the designed optical interfaces. The basic structural setup is the same as Figure 2d–f. a,b) The distribution of $|D_y|^2$ of excited hybrid surface waves, where D_y is the electric displacement field along the y direction. The coupling face of the Janus dipole is toward $+y$ direction if the rotation angle is $\theta = 0°$ but toward $-y$ direction if $\theta = 90°$. In addition, under this scenario, there is no excitation of linearly-polarized guided modes (including TM_0 and TM_1 guided modes). c,d) The distribution of $|D_y|^2$ of excited TM surface waves.

mal to the interface, as governed by the dispersion relation. To be specific, with the knowledge of Equation (6), we have:

$$H_y^{\text{hybrid,sw}}(x, y, z) = H_{y0}\left(k_{b,y}\varepsilon_a + k_{a,y}\varepsilon_b\right) \equiv 0 \tag{7}$$

where H_{y0} is a constant. This unique feature is numerically verified by the field distribution of the excited lowest-order surface waves in Figure 2d–f. This exotic feature of hybrid surface waves in the parallel-plate waveguide is fundamentally different from other types of hybrid TM-TE surface waves, such as chiral surface waves,[52–56] Dyakonov surface waves,[57–59] ghost surface polaritons,[60] hyperbolic shear polaritons,[61,62] whose field components are generally nonzero.

With the basic knowledge of hybrid surface waves, **Figure 3** numerically shows $|D_y|^2$ of a Janus dipole beyond polarization locking by the commercial finite element software of COMSOL Multiphysics, where D_y is the electric displacement field along the y direction. To avoid the emergence of higher-order hybrid TM-TE surface waves and guided modes, the working frequency in Figure 3 is chosen to be below the cut-off frequency of the TM_1 and TE_1 guided modes in the parallel-plate waveguide. This way, only the lowest-order hybrid TM-TE surface waves, and the fundamental guided mode TM_0 are present. To further eliminate the excitation of the fundamental guided mode, a negative-permittivity dielectric material (e.g., material *a*) is chosen to fill the region between the two out-couplers. On the other hand, a positive-permittivity dielectric environment (e.g., material *b*) with a spherical shape and a very small radius is designed to surround the Janus dipole, in order to enable the flipping of the coupling face. In addition, the distance between the two optical interfaces is set to be $2\ y_0 = \lambda_0/2$, which enables the efficient excitation of hybrid surface waves and avoids the coupling of surface waves supported by the two out-couplers, where λ_0 is the working wavelength of light in free space.

The orientation of the coupling face of the Janus dipole changes depending on the rotation angle. In Figure 3a, when the rotation angle is $\theta = 0°$, the coupling face is upward (toward the $+y$ direction). However, in Figure 3b, when $\theta = 90°$, the coupling face becomes downward (toward the y direction). For comparison, Figure 3c,d shows that the orientation of the coupling face remains unchanged for arbitrary rotation angle if the out-coupler supports linearly polarized TM surface waves.

Last but not least, we investigate the quantitative dependence of the coupling strength of a Janus dipole on the rotation angle. To be specific, $\gamma_{\pm,\text{hybrid/TM}} = |D_{\pm y_0}|^2/(|D_{+y_0}|^2 + |D_{-y_0}|^2)$ is plotted as a function of the rotation angle in **Figure 4**, where D_{+y_0} and D_{-y_0} are

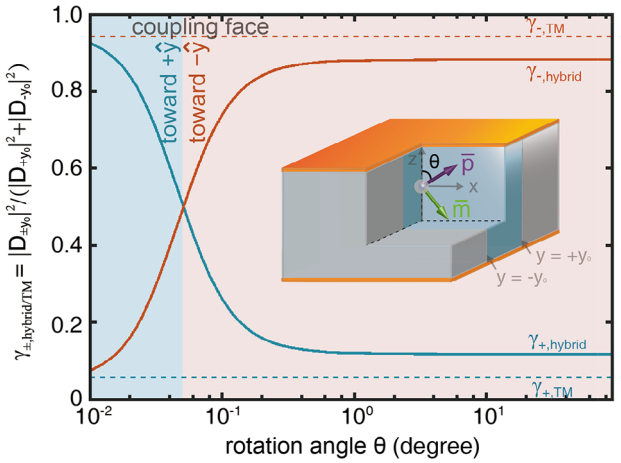

Figure 4. Dependence of the coupling face orientation of the Janus dipole on the rotation angle. Here we plot $\gamma_{\pm,\mathrm{hybrid/TM}} = |D_{\pm y_0}|^2/(|D_{+y_0}|^2+|D_{-y_0}|^2)$, which quantitatively characterizes the coupling strength, as a function of the rotation angle.

the electric displacement at the interface of $y = y_0$ and $y = -y_0$, respectively. Under the excitations of hybrid surface waves, if $\gamma_{+,\mathrm{hybrid}} \to 1$, the coupling face of the Janus dipole is upward (e.g., under the case of $\theta \to 0^\circ$ in Figure 4). If $\gamma_{+,\mathrm{hybrid}} \to 0$, the coupling face of the Janus dipole becomes downward (e.g., under the case of $\theta \to 90^\circ$ in Figure 4). Actually, the value of $\gamma_{+,\mathrm{hybrid}}$ ($\gamma_{-,\mathrm{hybrid}}$) would change from 0.93 (0.07) to 0.12 (0.88) when θ varies from 0° to 90°, which indicates the occurrence of the flipping between coupling and non-coupling faces. By contrast, under the excitations of linearly polarized surface waves, Figure 4 shows that $\gamma_{+,\mathrm{TM}} = 0.94$ and $\gamma_{-,\mathrm{TM}} = 0.06$ are insensitive to the variation of the rotation angle.

3. Conclusion

In conclusion, we have revealed a scheme to regulate the directional near-field coupling of Janus dipoles beyond polarization locking by exploiting hybrid TM-TE surface waves supported by the optical interface between different filling materials inside a parallel-plate waveguide. We have found that the coupling and non-coupling faces of a Janus dipole could be flipped by merely rotating the Janus dipole in a plane parallel to the designed optical interface, without resorting to the variation of the polarization state of excited surface waves. Essentially, this scheme for the manipulation of near-field coupling is enabled by the capability of hybrid surface waves to extract both TM and TE evanescent waves that the source carries. Looking forward, the interplay between various complex dipolar sources (e.g., chiral, circular, Huygens, and Janus dipoles) and hybrid surface waves (e.g., higher-order TM-TE surface waves, chiral surface waves, Dyakonov surface waves, ghost surface polaritons, and hyperbolic shear polaritons) requires continuing explorations, since it may further enrich the physics of dipole-matter interactions and facilitate the development of novel on-chip light sources.

Supporting Information

Supporting Information is available from the Wiley Online Library or from the author.

Acknowledgements

C.W. and Y.Z. contributed equally to this work. X.L. acknowledges the support partly from the National Natural Science Fund for Excellent Young Scientists Fund Program (Overseas) of China, the National Natural Science Foundation of China (NSFC) under Grant No. 62175212, Zhejiang Provincial Natural Science Fund Key Project under Grant No. LZ23F050003, and the Fundamental Research Funds for the Central Universities under Grant No. 226-2024-00022. H.C acknowledges the support partly from the Key Research and Development Program of the Ministry of Science and Technology under Grants No. 2022YFA1404704, 2022YFA1404902, and 2022YFA1405200, and the National Natural Science Foundation of China (NNSFC) under Grants No. 61975176, and the Key Research and Development Program of Zhejiang Province under Grant No.2022C01036, and the Fundamental Research Funds for the Central Universities. B.Z. acknowledges the support from the National Research Foundation Singapore Competitive Research Program no. NRF-CRP23-2019-0007, Singapore Ministry of Education Academic Research Fund Tier 3 under grant no. MOE2016-T3-1-006 and Tier 2 under grant no. MOE2019-T2-2-085. T.L acknowledges support from the NSF through UMN MRSEC under DMR-2011401

Conflict of Interest

The authors declare no conflict of interest.

Data Availability Statement

The data that support the findings of this study are available from the corresponding author upon reasonable request.

Keywords

hybrid TM-TE surface waves, Janus dipoles, near-field directionality, parallel-plate waveguides, polarization locking

Received: October 13, 2023
Revised: May 5, 2024
Published online: May 25, 2024

[1] Q. Ma, R. K. Kumar, S. Y. Xu, F. H. L. Koppens, J. C. W. Song, *Nat. Rev. Phys.* **2023**, *5*, 170.
[2] A. Kavokin, T. C. H. Liew, C. Schneider, P. G. Lagoudakis, S. Klembt, S. Hoefling, *Nat. Rev. Phys.* **2022**, *4*, 435.
[3] C. V. Rimoli, C. A. Valades-Cruz, V. Curcio, M. Mavrakis, S. Brasselet, *Nat. Commun.* **2022**, *13*, 301.
[4] M. Guan, M. Wang, K. Zhanghao, X. Zhang, M. Li, W. Liu, J. Niu, X. Yang, L. Chen, Z. Jing, M. Q. Zhang, D. Jin, P. Xi, J. Gao, *Light Sci. Appl.* **2022**, *11*, 4.
[5] D. Yao, P. H. He, H. C. Zhang, J. Zhu, M. Hu, T. J. Cui, *Prog. Electromagn. Res.* **2022**, *175*, 105.
[6] L. Liu, Z. Li, *Prog. Electromagn. Res.* **2022**, *173*, 93.
[7] Q. Zhang, G. Hu, W. Ma, P. Li, A. Krasnok, R. Hillenbrand, A. Alu, C. W. Qiu, *Nature* **2021**, *597*, 187.

[8] A. Forbes, M. de Oliveira, M. R. Dennis, *Nat. Photonics* **2021**, *15*, 253.
[9] T. L. Cocker, V. Jelic, R. Hillenbrand, F. A. Hegmann, *Nat. Photonics* **2021**, *15*, 558.
[10] M. Neugebauer, P. Wozniak, A. Bag, G. Leuchs, P. Banzer, *Nat. Commun.* **2016**, *7*, 11286.
[11] A. Andrea, B. Peter, N. Martin, L. Gerd, *Nat. Photonics* **2015**, *9*, 789.
[12] A. Rauschenbeutel, P. Schneeweiss, *Nat. Photonics* **2022**, *16*, 261.
[13] S. Wang, B. Hou, W. Lu, Y. Chen, Z. Q. Zhang, C. T. Chan, *Nat. Commun.* **2019**, *10*, 832.
[14] S. H. Gong, F. Alpeggiani, B. Sciacca, E. C. Garnett, L. Kuipers, *Science* **2018**, *359*, 443.
[15] P. Xi, X. Wei, J. Qu, V. V. Tuchin, *Light Sci. Appl.* **2022**, *11*, 156.
[16] A. Qu, M. Sun, J. Y. Kim, L. Xu, C. Hao, W. Ma, X. Wu, X. Liu, H. Kuang, N. A. Kotov, C. Xu, *Nat. Biomed. Eng.* **2021**, *5*, 103.
[17] X. Wang, Y. Wang, W. Gao, L. Song, C. Ran, Y. Chen, W. Huang, *Adv. Mater.* **2021**, *33*, 2003615.
[18] J. S. Lee, N. Farmakidis, C. D. Wright, H. Bhaskaran, *Sci. Adv.* **2022**, *8*, eabn9459.
[19] Y. Long, J. Ren, Z. Guo, H. Jiang, Y. Wang, Y. Sun, H. Chen, *Phys. Rev. Lett.* **2020**, *125*, 157401.
[20] D. O'Connor, P. Ginzburg, F. J. Rodriguez-Fortuno, G. A. Wurtz, A. V. Zayats, *Nat. Commun.* **2014**, *5*, 5327.
[21] P. V. Kapitanova, P. Ginzburg, F. J. Rodriguez-Fortuno, D. S. Filonov, P. M. Voroshilov, P. A. Belov, A. N. Poddubny, Y. S. Kivshar, G. A. Wurtz, A. V. Zayats, *Nat. Commun.* **2014**, *5*, 3226.
[22] T. Shegai, S. Chen, V. D. Miljkovic, G. Zengin, P. Johansson, M. Kall, *Nat. Commun.* **2011**, *2*, 481.
[23] B. Xiong, Y. Liu, Y. Xu, L. Deng, C. W. Chen, J. N. Wang, R. Peng, Y. Lai, Y. Liu, M. Wang, *Science* **2023**, *379*, 294.
[24] T. Guo, Z. Lin, X. Xu, Z. Zhang, X. Chen, N. He, G. Wang, Y. Jin, J. Evans, S. He, *Prog. Electromagn. Res.* **2023**, *177*, 43.
[25] M. Matsubara, T. Kobayashi, H. Watanabe, Y. Yanase, S. Iwata, T. Kato, *Nat. Commun.* **2022**, *13*, 6708.
[26] I. Kim, J. Jang, G. Kim, J. Lee, T. Badloe, J. Mun, J. Rho, *Nat. Commun.* **2021**, *12*, 3614.
[27] Y. Jiang, X. Lin, H. Chen, *Prog. Electromagn. Res.* **2021**, *170*, 169.
[28] L. Deng, J. Deng, Z. Guan, J. Tao, Y. Chen, Y. Yang, D. Zhang, J. Tang, Z. Li, Z. Li, S. Yu, G. Zheng, H. Xu, C. W. Qiu, S. Zhang, *Light Sci. Appl.* **2020**, *9*, 101.
[29] X. Lin, B. Zhang, *Laser Photonics Rev* **2019**, *13*, 1900081.
[30] X. Shi, X. Lin, I. Kaminer, F. Gao, Z. Yang, J. D. Joannopoulos, M. Soljačić, B. Zhang, *Nat. Phys.* **2018**, *14*, 1001.
[31] Y. Jiang, X. Lin, T. Low, B. Zhang, H. Chen, *Laser Photonics Rev* **2018**, *12*, 1800049.
[32] A. Pors, M. G. Nielsen, T. Bernardin, J. C. Weeber, S. I. Bozhevolnyi, *Light Sci. Appl.* **2014**, *3*, e197.
[33] Y. Li, Z. Zhang, H. Chen, F. Gao, *Prog. Electromagn. Res.* **2023**, *178*, 37.
[34] M. F. Picardi, C. P. T. McPolin, J. J. Kingsley-Smith, X. Zhang, S. Xiao, F. J. Rodríguez-Fortuño, A. V. Zayats, *Appl. Phys. Rev.* **2022**, *9*, 021410.
[35] J. Lin, J. P. B. Mueller, Q. Wang, G. Yuan, N. Antoniou, X. C. Yuan, F. Capasso, *Science* **2013**, *340*, 331.
[36] F. J. Rodriguez-Fortuno, G. Marino, P. Ginzburg, D. O'Connor, A. Martinez, G. A. Wurtz, A. V. Zayats, *Science* **2013**, *340*, 328.
[37] S. Y. Lee, I. M. Lee, J. Park, S. Oh, W. Lee, K. Y. Kim, B. Lee, *Phys. Rev. Lett.* **2012**, *108*, 213907.
[38] X. Chen, L. Huang, H. Muhlenbernd, G. Li, B. Bai, Q. Tan, G. Jin, C. W. Qiu, S. Zhang, T. Zentgraf, *Nat. Commun.* **2012**, *3*, 1198.
[39] M. F. Picardi, A. V. Zayats, F. J. Rodríguez-Fortuño, *Phys. Rev. Lett.* **2018**, *120*, 117402.
[40] M. F. Picardi, M. Neugebauer, J. S. Eismann, G. Leuchs, P. Banzer, F. J. Rodríguez-Fortuño, A. V. Zayats, *Light Sci. Appl.* **2019**, *8*, 52.
[41] Y. Zhong, C. Wang, C. Bian, X. Chen, J. Chen, X. Zhu, H. Hu, T. Low, S. Dai, H. Chen, B. Zhang, X. Lin, *Opt. Lett.* **2024**, *49*, 4.
[42] Y. Zhong, X. Lin, J. Jiang, Y. Yang, G. G. Liu, H. Xue, T. Low, H. Chen, B. Zhang, *Laser Photonics Rev* **2021**, *15*, 2000388.
[43] M. F. Picardi, A. M. A. V. Zayats, F. J. Rodríguez-Fortuño, *Phys. Rev. B* **2017**, *95*, 245416.
[44] M. Kerker, D. S. Wang, C. L. Giles, *J. Opt. Soc. Am.* **1983**, *73*, 765.
[45] S. Nechayev, J. S. Eismann, M. Neugebauer, P. Wozniak, A. Bag, G. Leuchs, P. Banzer, *Phys. Rev. A* **2019**, *99*, 041801.
[46] X. Zhang, J. Chen, R. Chen, C. Wang, T. Cai, R. Abdi-Ghaleh, H. Chen, X. Lin, *ACS Photonics* **2023**, *10*, 2102.
[47] O. Y. Yermakov, A. A. Hurshkainen, D. A. Dobrykh, P. V. Kapitanova, I. V. Iorsh, S. B. Glybovski, A. A. Bogdanov, *Phys. Rev. B* **2018**, *98*, 195404.
[48] F. Ding, *Prog. Electromagn. Res.* **2022**, *174*, 55.
[49] O. Y. Yermakov, V. Lenets, A. Sayanskiy, J. Baena, E. Martini, S. Glybovski, S. Maci, *Phys. Rev. X* **2021**, *11*, 031038.
[50] Y. Liang, H. Lin, S. Lin, J. Wu, W. Li, F. Meng, Y. Yang, X. Huang, B. Jia, Y. Kivshar, *Nano Lett* **2021**, *21*, 8917.
[51] P. Huo, S. Zhang, Y. Liang, Y. Lu, T. Xu, *Adv. Opt. Mater.* **2019**, *7*, 1801616.
[52] T. Huang, X. Tu, C. Shen, B. Zheng, J. Wang, H. Wang, K. Khaliji, S. H. Park, Z. Liu, T. Yang, Z. Zhang, L. Shao, X. Li, T. Low, Y. Shi, X. Wang, *Nature* **2022**, *605*, 63.
[53] J. Cai, W. Zhang, L. Xu, C. Hao, W. Ma, M. Sun, X. Wu, X. Qin, F. M. Colombari, A. F. de Moura, J. Xu, M. C. Silva, E. B. Carneiro-Neto, W. R. Gomes, R. A. L. Vallee, E. C. Pereira, X. Liu, C. Xu, R. Klajn, N. A. Kotov, H. Kuang, *Nat. Nanotechnol.* **2022**, *17*, 408.
[54] J. Chen, X. Lin, M. Chen, T. Low, H. Chen, S. Dai, *Appl. Phys. Lett.* **2021**, *119*, 240501.
[55] X. Lin, Z. Liu, T. Stauber, G. Gomez-Santos, F. Gao, H. Chen, B. Zhang, T. Low, *Phys. Rev. Lett.* **2020**, *125*, 077401.
[56] S. S. Sunku, G. X. Ni, B. Y. Jiang, H. Yoo, A. Sternbach, A. S. McLeod, T. Stauber, L. Xiong, T. Taniguchi, K. Watanabe, P. Kim, M. M. Fogler, D. N. Basov, *Science* **2018**, *362*, 1153.
[57] H. Hu, X. Lin, L. J. Wong, Q. Yang, D. Liu, B. Zhang, Y. Luo, *eLight* **2022**, *2*, 2.
[58] O. Takayama, D. Artigas, L. Torner, *Nat. Nanotechnol.* **2014**, *9*, 419.
[59] M. I. Dyakonov, *J. Exp. Theor. Phys.* **1988**, *94*, 119.
[60] W. Ma, G. Hu, D. Hu, R. Chen, T. Sun, X. Zhang, Q. Dai, Y. Zeng, A. Alu, C. W. Qiu, P. Li, *Nature* **2021**, *596*, 362.
[61] G. Hu, W. Ma, D. Hu, J. Wu, C. Zheng, K. Liu, X. Zhang, X. Ni, J. Chen, X. Zhang, Q. Dai, J. D. Caldwell, A. Paarmann, A. Alu, P. Li, C. W. Qiu, *Nat. Nanotechnol.* **2023**, *18*, 64.
[62] N. C. Passler, X. Ni, G. Hu, J. R. Matson, G. Carini, M. Wolf, M. Schubert, A. Alu, J. D. Caldwell, T. G. Folland, A. Paarmann, *Nature* **2022**, *602*, 595.
[63] J. A. Kong, *Electromagnetic Wave Theory*, EMW, Cambridge, MA, USA, **2007**.
[64] C. Bian, Y. Zhong, X. Chen, T. Low, H. Chen, B. Zhang, X. Lin, *Phys. Rev. A* **2024**, *109*, 033505.